Available online at www.sciencedirect.com
SCIENCE DIRECT®
Journal of Sound and Vibration 274 (2004) 53–72
JOURNAL OF SOUND AND VIBRATION
www.elsevier.com/locate/jsvi

Transient vibration of smart structures using a coupled piezoelectric-mechanical theory

R.P. Thornburgh*, A. Chattopadhyay, A. Ghoshal

Department of Mechanical and Aerospace Engineering, Arizona State University, Tempe, AZ 85287-6106, USA

Received 29 July 2002; accepted 13 May 2003

Abstract

A smart structural model is developed to analytically determine the transient response of arbitrary structures with piezoelectric materials and attached electrical circuitry. The equations of motion are formulated using a coupled piezoelectric formulation solving for strain and electric charge. The composite host structure is modelled using a refined higher-order laminate theory and additional degrees of freedom are then added to describe any attached electrical circuitry. The developed model results in a general framework that can be useful in solving a wide variety of coupled piezoelectric-mechanical problems. A comparison is made with classical plate theory and uncoupled piezoelectric modelling techniques to illustrate the importance of proper modelling in order to accurately estimate sensor response during transient loading of adaptive structures. The model is compared with experimental results, showing the model to be capable of capturing several effects not possible with traditional smart structures modelling techniques.

1. Introduction

Piezoelectric materials such as lead zirconate titanate (PZT) are becoming more widely used in conjunction with control systems to damp out vibrations in structures. These ''smart'' structures use PZTs to both senses, strain in the structure and to create localized forces to counter the vibration. Strain present in the piezoelectric sensor induces an electric field in the material and sensing is accomplished by either measuring the voltage or the charge output of the sensor electrodes. To use the PZT as an actuator, a voltage can be applied to the electrodes inducing an electric field, and in turn, a stress within the PZT.

*Corresponding author. NASA Langley Research Center, M/S 188B, Hamptin, VA 23681-2199, USA.
E-mail address: robert.p.thornburgh@nasa.gov (R.P. Thornburgh).

0022-460X/$ - see front matter
doi:10.1016/S0022-460X(03)00648-5

Analysis of smart structures using piezoelectric materials as either sensors or actuators has traditionally been performed using uncoupled models [1,2]. Uncoupled models make the assumption that the electric field within the piezoelectric material is constant and proportional to the ratio of electrode voltage to PZT thickness. Having made this assumption, the strain induced by an actuator is modelled with a single uncoupled equation and the charge output of a sensor is described by another uncoupled equation. This makes analysis of a smart structure relatively simple, but this method has its limitations. The mechanical and electric response of a piezoelectric device is in reality described by a pair of coupled equations [3] and cannot be accurately modelled if treated independently. It is therefore necessary to simultaneously solve for both the electric response as well as the mechanical response regardless of whether the PZT is being used as a sensor or actuator. Also, the uncoupled model is not capable of taking into consideration any electrical circuitry connected to the piezoelectric device. This has been recognized in some specific applications and coupled equations have been used to model passive damping circuits [4,5] and develop self-sensing actuators [6]. Only recently have the coupled equations been simultaneously used for general-purpose analysis of adaptive structures [7–9].

In general, the errors that result from using uncoupled models, as opposed to coupled ones, are relatively moderate. However, there are some cases in which very large differences exist when using the two approaches. One such case is for high frequency vibrations or thick piezoelectric material. The objective of this work is to demonstrate the importance of proper modelling methods when analyzing high frequency vibration in smart composite structures and to show a comparison between the results predicted by uncoupled and coupled approaches.

2. Mathematical theory

The model developed in this paper is based on a coupled piezoelectric-mechanical formulation, which allows accurate prediction of both the mechanical and the electrical response of a piezoelectric structural system. A higher-order theory is used to model the transverse shear effects, which are critical in anisotropic laminates of arbitrary thickness. A non-linear time integration technique is used to predict the transient response of the structure. This time integration method is based on the Newmark-beta method with Newton–Raphson (NR) iteration. The procedure is implemented using a finite element solution technique.

A recently developed two-way coupled piezoelectric-mechanical theory [9] is used to model composite plates with piezoelectric actuators. The construction of a model for smart composite laminates starts with the formulation of the constitutive relations. Traditionally these are expressed as a function of the components of strain (ε_{ij}) and electric field (E_i) as follows

$$\sigma_{ij} = c^E_{ijkl}\varepsilon_{kl} - e_{kij}E_k, \quad D_i = e_{ikl}\varepsilon_{kl} + \chi^S_{ik}E_k, \tag{1,2}$$

where σ_{ij} and D_i are the components of the mechanical stress and the electrical displacement, and c^E_{ijkl}, e_{ijk}, and χ^S_{ik} are the elastic, piezoelectric, and dielectric permittivity constants, respectively. It should be noted that the elastic constants used correspond to the zero electric field values (PZT is shorted out) and the dielectric permittivities correspond the zero strain values (clamped). Eq. (1) is often referred to as the converse effect and Eq. (2) is known as the direct effect. These equations are traditionally used due to the ease with which piezoelectric materials can be modelled as either

actuators or sensors. Most formulations make the assumption, based on the geometry of thin, electroded piezoelectrics, that the electric field is constant through the thickness of the material and zero within the plane of the piezoelectric device. However, if the strain is not constant through the thickness of the piezoelectric material, such as in the case of bending or transverse shear, then this method results in electric displacement varying through the thickness. This also implies differing amounts of charge on the upper and lower electrodes, which is a violation of the conservation of charge principle. This has been resolved by making the electric potential, and in turn the electric field, high order functions through the thickness co-ordinate to match the displacement and strain fields in the structure. However, such an approach leads to additional degrees of freedom to describe the electric potential. Another drawback of such an approach is that the resulting system matrices in finite element implementation are not symmetric. This results in a sizable increase in the computational effort required to solve the system of equations.

To address these issues, a different approach is used, in which Eqs. (1) and (2) are reformulated in terms of the mechanical strain and the electric displacement as

$$\sigma_{ij} = c^D_{ijkl}\varepsilon_{kl} - h_{kij}D_k, \quad E_i = -h_{ikl}\varepsilon_{kl} + \beta^S_{ik}D_k, \tag{3,4}$$

where c^D_{ijkl}, e_{ijk}, and β^S_{ik} are the open circuit elastic and zero strain dielectric constants, respectively. The coefficient h_{ijk} now represents the coupling between the strain and the electric displacement. In matrix form these are written as

$$\sigma = \mathbf{C}^D\varepsilon - \mathbf{hD}, \;\; \mathbf{E} = -\mathbf{h}^{\mathrm{T}}\varepsilon + \boldsymbol{\beta}^S\mathbf{D}. \tag{5,6}$$

Using this formulation, the electric displacement ($\mathbf{D}$) can be taken as constant through the thickness of the PZT, thus ensuring conservation of charge on each of the electrodes.

The equations of motion can be formulated using a variational approach and Hamilton's Principle [3]. The variational principle between times t_o and t, for the piezoelectric body of volume V can be written as

$$\delta\Pi = 0 = \int_{t_o}^{t}\int_V \left[\delta\left(\tfrac{1}{2}\rho\dot{\mathbf{u}}^{\mathrm{T}}\dot{\mathbf{u}}\right) - \delta\mathbf{H}(\varepsilon,\mathbf{D})\right] \mathrm{d}V\,\mathrm{d}t + \int_{t_o}^{\mathrm{t}} \delta\mathbf{W}\,\mathrm{d}t, \tag{7}$$

where the first term represents the kinetic energy, the second term the electric enthalpy, and $\delta\mathbf{W}$ is the total virtual work done on the structure. The terms $\mathbf{u}$ and ρ refer to the mechanical displacement and density, respectively. The electric enthalpy is given by

$$\mathbf{H}(\varepsilon,\mathbf{D}) = \tfrac{1}{2}\varepsilon^{\mathrm{T}}\mathbf{C}^D\varepsilon - \varepsilon^{\mathrm{T}}\mathbf{hD} + \tfrac{1}{2}\mathbf{D}^{\mathrm{T}}\boldsymbol{\beta}^S\mathbf{D}. \tag{8}$$

The work done by body forces ($\mathbf{f}_B$), surface tractions ($\mathbf{f}_S$), and electrical potential (ϕ) applied to the surface of the piezoelectric material can be expressed by

$$\delta\mathbf{W} = \int_V \delta\mathbf{u}^{\mathrm{T}}\mathbf{f}_B\,\mathrm{d}V + \int_S \delta\mathbf{u}^{\mathrm{T}}\mathbf{f}_S\mathrm{d}S + \int_S \delta\mathbf{D}^{\mathrm{T}}\phi\,\mathrm{d}S. \tag{9}$$

Eqs. (7–9) provide the equations of motion for the piezoelectric body. To solve them, assumptions must be made concerning the nature of the mechanical strain and the electrical displacement. First, it is assumed that the piezoelectric material is oriented with its polarization axis normal to the plane of the plate and that the PZT has electrodes covering its upper and lower surfaces. This is the usual geometry for transversely operating piezoelectric actuators and sensors which are bonded to the surface or embedded in plate structures. For this case, the electric

displacement becomes zero along the two in-plane directions. The out-of-plane electric displacement can then be discretized over the surface of the piezoelectric device using finite elements.

A refined higher-order laminate theory [10] is used to model the mechanical displacement field. The laminate is assumed to be a plate structure composed of an arbitrary number of orthotropic lamina arranged with varying orientations. The co-ordinate system for the plate is taken to be with the $x-y$ plane parallel to the plane of the plate and the z co-ordinate normal to the plane of the plate measured from the center. The refined higher-order theory assumes a parabolic distribution of transverse shear strain, thus providing accurate estimation of transverse shear stresses for moderately thick laminates with little increase in computational effort. The theory starts with a general third order displacement field and is simplified by imposing the stress free boundary conditions on the free surfaces. Since the laminate is orthotropic, this implies that the transverse shear strains are zero. The refined displacement field now takes the following form

$$\mathbf{u}_1 = u + z\left(\psi_x - \frac{\partial w}{\partial x}\right) - \frac{4z^3}{3h^2}\psi_x, \quad \mathbf{u}_2 = v + z\left(\psi_y - \frac{\partial w}{\partial y}\right) - \frac{4z^3}{3h^2}\psi_y, \quad \mathbf{u}_3 = w, \tag{10a–c}$$

where u, v, and w are the displacements of the midplane, and the parameters ψ_x and ψ_y are the rotations of the normal at $z = 0$ about the y and x axes, respectively. Note that u, v, w, ψ_x and ψ_y are all functions of the x and y co-ordinates only. The variable z represents the location with respect to the midplane of the plate, and h is the total plate thickness. The coupled piezoelectric-mechanical theory can be developed using other plate theories, but the chosen plate model affects the constraints imposed on the delamination boundaries developed later in this paper.

By using the above equations and the finite element method, the governing equations can be written in matrix form as

$$\begin{bmatrix} \mathbf{M}_u & 0 \\ 0 & 0 \end{bmatrix} \begin{Bmatrix} \ddot{\mathbf{u}}_e \\ \ddot{\mathbf{D}} \end{Bmatrix} + \begin{bmatrix} \mathbf{C}_u & 0 \\ 0 & 0 \end{bmatrix} \begin{Bmatrix} \dot{\mathbf{u}}_e \\ \dot{\mathbf{D}} \end{Bmatrix} + \begin{bmatrix} \mathbf{K}_{uu} & \mathbf{K}_{uD} \\ \mathbf{K}_{Du} & \mathbf{K}_{DD} \end{bmatrix} \begin{Bmatrix} \mathbf{u}_e \\ \mathbf{D} \end{Bmatrix} = \begin{Bmatrix} \mathbf{F}_u \\ \mathbf{F}_D \end{Bmatrix}, \tag{11}$$

where $\mathbf{u}_e$ is the nodal displacements, $\mathbf{D}$ is the vector of the PZT nodal electrical displacements. The matrix $\mathbf{M}_u$ is the structural mass matrix and $\mathbf{C}_u$ is the structural damping matrix. The matrix $\mathbf{K}_{uu}$ is the mechanical stiffness matrix, $\mathbf{K}_{DD}$ is the electrical stiffness matrix, and $\mathbf{K}_{uD}$ and $\mathbf{K}_{Du}$ are the stiffness matrices due to piezoelectric-mechanical coupling. The vectors $\mathbf{F}_u$ and $\mathbf{F}_D$ are the force vectors due to mechanical and electrical loading. To incorporate structural damping into the equations, a structural damping matrix $\mathbf{C}_u$ is added. The nature of the damping matrix can be chosen to meet the needs of the user.

The absence of any electrical inertia or damping terms in Eq. (11) is a result of only considering the mechanical aspects of the smart structure. When considering an integrated smart structural system as a whole, additional terms must be added for electrical components in the system. For a simple LRC circuit, the variational energy can be calculated based on the charge flow in the circuit, q, as follows:

$$\delta\mathbf{\Pi}_q = \delta\left(\frac{1}{2}L\dot{q}^2\right) - \delta q R\dot{q} - \delta\left(\frac{1}{2C}q^2\right) + V\delta q, \tag{12}$$

where L, R, C and V are the inductance, resistance, capacitance and applied voltage. The importance of formulating Hamilton's Principle in terms of the charge, rather than electric field or

potential, now becomes apparent. If the equations of motion for any electrical system attached to the smart structure can be formulated in the following form

$$\mathbf{M}_q\ddot{\mathbf{q}}_e + \mathbf{C}_q\dot{\mathbf{q}}_e + \mathbf{K}_q\mathbf{q}_e = \mathbf{F}_q. \tag{13}$$

These equations can then be combined with Eq. (11). However, Eq. (11) is formulated in terms of electric displacement (charge flow per unit area) as opposed to total charge flow ($\mathbf{q}_e$) in the circuit. These two quantities can be related by integration of the electric displacement over the surface area of the piezoelectric device as

$$q_i = \left(\int_S \mathbf{N}_q \, \mathrm{d}S\right)\mathbf{D}_{ie} \;\text{ or }\; \mathbf{q}_e = \mathbf{A}_q\mathbf{D}_e. \tag{14}$$

Since the finite element method is used, the integration of the shape functions, $\mathbf{N}_q$, leads to the formation of a simple matrix operator, $\mathbf{A}_q$, which relates nodal electric displacement to total charge flow. Combining Eqs. (24) and (26), the resulting coupled electrical-mechanical system equations are obtained:

$$\begin{bmatrix} \mathbf{M}_u & 0 \\ 0 & \mathbf{A}_q^{\mathrm{T}}\mathbf{M}_q\mathbf{A}_q \end{bmatrix} \begin{Bmatrix} \ddot{\mathbf{u}}_e \\ \ddot{\mathbf{D}}_e \end{Bmatrix} + \begin{bmatrix} \mathbf{C}_u & 0 \\ 0 & \mathbf{A}_q^{\mathrm{T}}\mathbf{C}_q\mathbf{A}_q \end{bmatrix} \begin{Bmatrix} \dot{\mathbf{u}}_e \\ \dot{\mathbf{D}}_e \end{Bmatrix} + \begin{bmatrix} \mathbf{K}_{uu} & \mathbf{K}_{uD} \\ \mathbf{K}_{Du} & \mathbf{K}_{DD} + \mathbf{A}_q^{\mathrm{T}}\mathbf{K}_q\mathbf{A}_q \end{bmatrix} \begin{Bmatrix} \mathbf{u}_e \\ \mathbf{D}_e \end{Bmatrix} = \begin{Bmatrix} \mathbf{F}_u \\ \mathbf{F}_\mathbf{D} \end{Bmatrix}, \tag{15}$$

where $\mathbf{q}_e$ includes not only the charge associated with the piezoelectric device, but also the electrical system.

To model a particular sensor configuration the electrical circuit must be modelled or appropriate electrical boundary conditions must be applied. If sensor charge flow is being measured, then the voltage is specified as zero. If sensor voltage is being measured, then the net charge flow, Eq. (14), is specified as zero.

The non-linear transient analysis is conducted using Newmark-beta method with NR iteration [11]. This results in a time integration method that can be iterated at each time step to provide accurate prediction of the transient response of the system.

3. Piezoelectric modelling results

The developed model is used to calculate the response of a composite plate with surface bonded actuators subjected to impulse loading. The objective is to demonstrate the nature and magnitude of errors that exist when simpler approaches are used. First, a comparison is made between the response predicted by the refined higher-order laminate theory and the classical plate theory. Then the difference between the coupled piezoelectric-mechanical model and the uncoupled model is examined.

The plate to be modelled is assumed to be clamped at one end with a cantilevered section 31.1 cm long by 5.1 cm wide. The plate is modelled as a graphite-epoxy laminate with 16 plies of 0.137 mm ply thickness. A variety of ply stacking sequences are considered, including cross-ply as well as balanced and unbalanced angle-ply lay-ups. A piezoelectric patch is assumed to be bonded

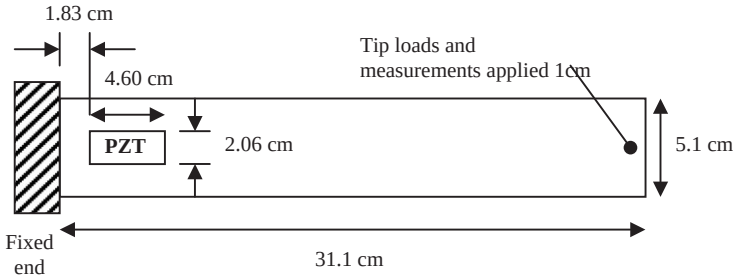

Fig. 1. Cantilever plate layout.

Table 1
List of material properties used

Material property	Graphite-epoxy	PZT-5H
E_1 (GPa)	372.0	60.6
E_2 (GPa)	4.12	60.6
v_{12}	0.275	0.29
v_{23}	0.42	0.48
G_{12} (GPa)	3.99	23.49
G_{23} (GPa)	3.6	22.99
ρ (kg/m^3)	1788.5	7500
d_{31} and d_{32} (nm/V)	n/a	−0.274
d_{24} and d_{15} (nm/V)	n/a	0.741
χ_{33}^{T} (nF/m)	n/a	30.1

to the upper surface of the plate as shown in Fig. 1. The patch is modelled as PZT-5 H with a thickness of 0.25 mm. The material properties used for the graphite-epoxy and PZT are listed in Table 1.

3.1. Higher-order versus classical plate theory

First, a comparison is made between models using the refined higher-order laminate theory and the classical plate theory. By including transverse shear stress, the refined higher-order theory has been shown to result in a model with lower natural frequencies than those predicted by the classical plate theory [10]. This reduction in natural frequencies is due to the fact that during vibration the plate undergoes not only pure bending, but also deformation in the form of out-of-plane shear. The bending modes are all composed of both forms of deformation and thus, models that do not include both are too stiff. The effects are not only more significant for thicker laminates, but also create larger changes in out-of-plane modes with higher natural frequencies.

A laminate stacking sequence of $[0^\circ, 90^\circ]_{4s}$ is considered first, with the PZT modelled as being open circuited. This laminate has a ratio of plate length to thickness of 142, making this a relatively thin plate. The plate is modelled with the refined higher-order laminate theory, which includes the effects of transverse shear, as well as with the classical plate theory, which neglect transverse shear. All other aspects of the modelling are identical in both cases. The plate is

simulated as being subjected to a 5-N, 1 μs impulse point load at the tip. The analysis is performed for both cases with a 1 μs time step. Fig. 2 shows the resulting tip displacement obtained by using the two models. The difference between the higher-order theory and the classical theory is modest, but noticeable during the short time interval analyzed, even for this thin laminate. The electrical response of the system can be seen in Fig. 3, which shows the predicted voltage output from the PZT sensor during the impulse loading. A much more noticeable difference in voltage output is observed between the two plate theories in comparison to the modest difference in tip displacement. Although the shape of the response is very similar, the magnitude of the signal differs significantly. It is difficult to quantify the effect of the plate theory on the electrical response. The change in the natural frequencies of the plate contributes to the change in sensor output, but also transverse shear itself generates an internal electrical potential within the piezoelectric device due to the existence of the d_{24} and d_{15} piezoelectric constants seen in Table 1.

Next, the same plate is analyzed for a 1 N, 5 μs impulse point load at the tip. The time step for the transient analysis is 5 μs, so that a longer time segment could be examined. The tip

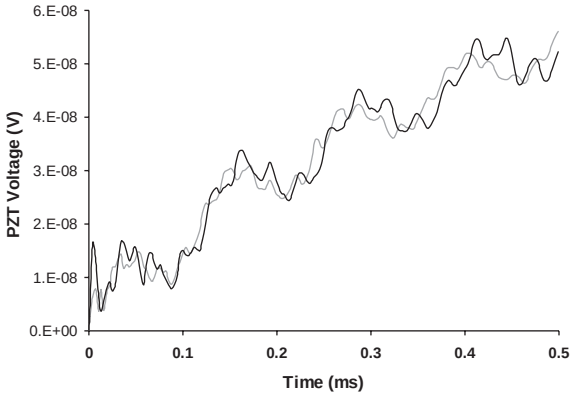

Fig. 2. Tip displacement for $[0^\circ, 90^\circ]_{4s}$ laminate ($L/h = 142$) under 1 μs impulse loading; classical plate theory (——), and higher-order plate theory (——).

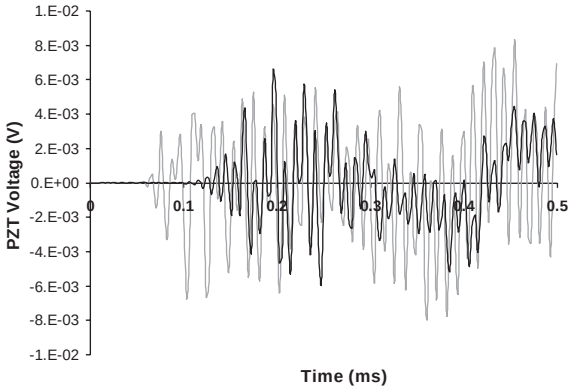

Fig. 3. Sensor output for $[0^\circ, 90^\circ]_{4s}$ laminate ($L/h = 142$) under 1 μs impulse loading; classical plate theory (——), and higher-order plate theory (——).

displacement for the higher-order and classical plate theories is shown in Fig. 4 and the sensor output is shown in Fig. 5. When a longer time step is used, 5 μs as opposed to 1 μs, the differences between the two theories are much less significant for the thin plate, because the transverse shear has less influence on the lower order modes. Note that in this case the charge flow from the PZT is estimated for sensor output. It can be seen that the difference in the way transverse shear is modelled by the two-plate theories affects sensor charge flow to a greater degree than tip displacement.

An increase in plate thickness increases the influence of transverse shear on the response of the plate, and thus, the difference in the response predicted by the higher-order theory and the classical plate theory should increase as well. This is shown in Fig. 6, which depicts the tip response for a $[0_5^\circ, 90_5^\circ]_{4s}$ laminate. The ratio of plate length to thickness is 28.4 for this case, making this a moderately thick plate. The impulse length and time step used in this case are both 1 μs. By increasing plate thickness, difference in natural frequencies predicted by the classical plate

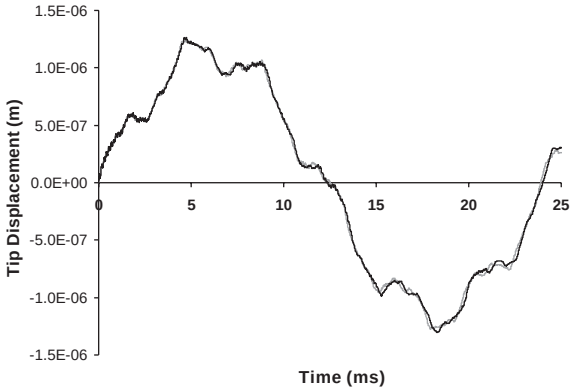

Fig. 4. Tip displacement for $[0^\circ, 90^\circ]_{4s}$ laminate ($L/h = 142$) under 5 μs impulse loading; classical plate theory (——), and higher-order plate theory (——).

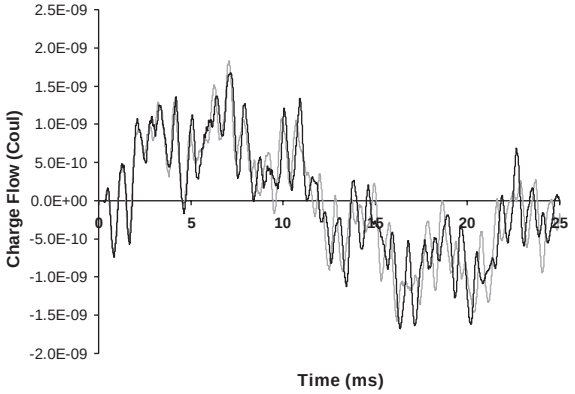

Fig. 5. Sensor output for $[0^\circ, 90^\circ]_{4s}$ laminate ($L/h = 142$) under 5 μs impulse loading; classical plate theory (——), and higher-order plate theory (——).

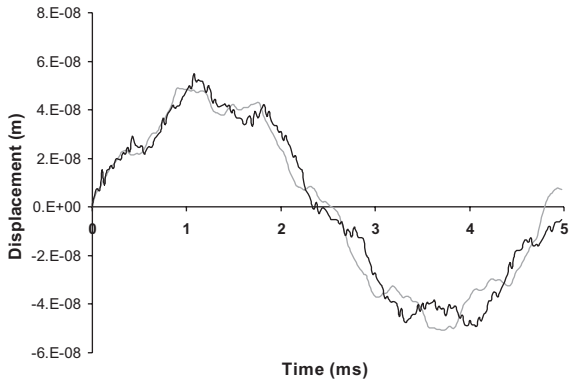

Fig. 6. Tip displacement for $[0_5^\circ, 90_5^\circ]_{4s}$ laminate ($L/h = 28.4$) under 1 μs impulse loading; classical plate theory (——), and higher-order plate theory (——).

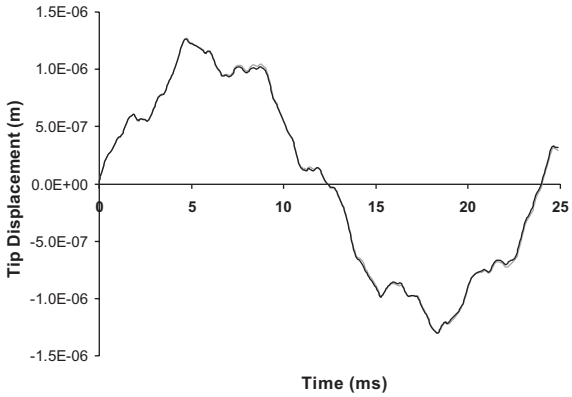

Fig. 7. Tip displacement for $[0^\circ, 90^\circ]_{4s}$ laminate under impulse loading; uncoupled model (——), and coupled model (——).

theory and the higher-order plate theory become greater, resulting in sizable differences in plate deflections.

3.2. Coupled versus uncoupled piezoelectric theory

Next a comparison is made between the coupled and the uncoupled piezoelectric models. The plate with $[0^\circ, 90^\circ]_{4s}$ stacking sequence is considered. The plate is simulated being subjected to a 1 N, 5 μs impulse point load at the tip, and a 5 μs time step is used for the transient analysis. The PZT is assumed to be open circuited and voltage is computed for sensor output. The response is calculated using both the coupled theory presented in this work as well as the traditional uncoupled approach. The resulting tip displacement is shown in Fig. 7 for both approaches. Only very slight differences between the two models are observed in this case. This is due to the relatively small size of the PZT patch and its limited contribution to the overall plate stiffness. Though the difference might be expected to be larger for thicker PZT patches, the displacement is

more greatly influenced by the plate theory as opposed to the piezoelectric model. Fig. 8 shows the voltage output of the sensor for both cases. Here it can be seen that the coupled theory predicts dramatically different results from the uncoupled approach, even though the displacements are shown to be similar. Fig. 9 presents the output if the charge flow from the PZT is instead measured. Again the coupled theory predictions greatly differ from the uncoupled approach.

The reason for the large differences in the electrical response is due to the fact that the uncoupled theory assumes that the electric field is constant over the entire area of the PZT. During impulse loading high frequency bending waves travel across the length of the plate, as shown in Fig. 10. As these high frequency waves move across the PZT, the piezoelectric material is subjected to areas of local compression and tension. As a result, the electric displacement is positive in some local areas and negative in others as shown in Fig. 11. The net charge output is thereby reduced since charge merely flows from one region of the patch to another. When the PZT is open circuited, the charge flow within the PZT still occurs making the voltage output very sensitive to local strain. As shown in Fig. 12, the strains at the two ends of the PZT are very dissimilar during the impulse loading. Thus, there exists a continuously changing strain gradient

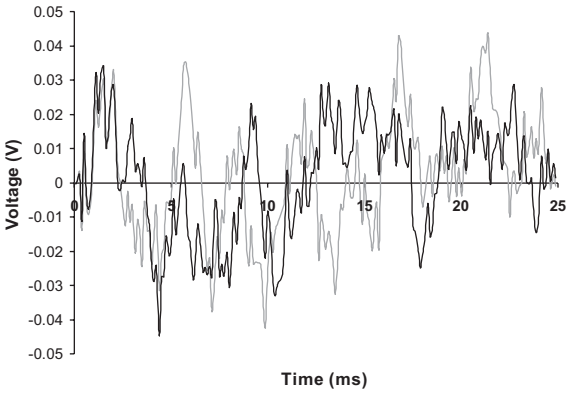

Fig. 8. Sensor output for $[0^\circ, 90^\circ]_{4s}$ laminate under impulse loading; uncoupled model (——), and coupled model (——).

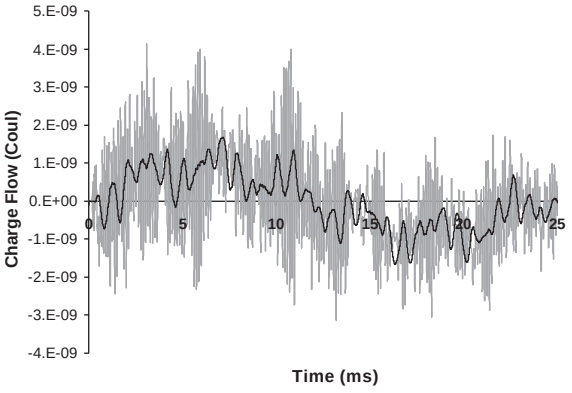

Fig. 9. Sensor charge flow for $[0^\circ, 90^\circ]_{4s}$ laminate under impulse loading; uncoupled model (——), and coupled model (——).

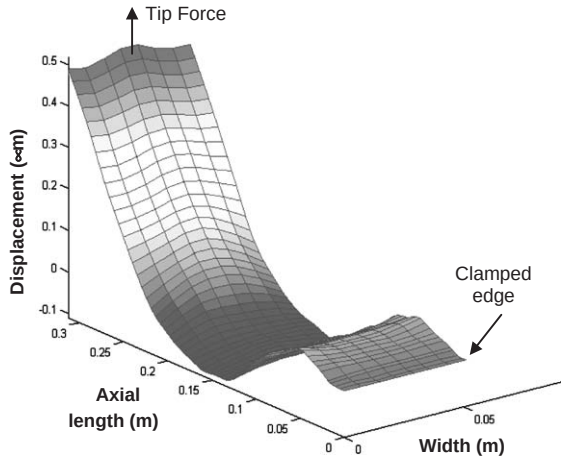

Fig. 10. Plate displacement at $t = 73.95\,\mu s$ during impulse tip loading.

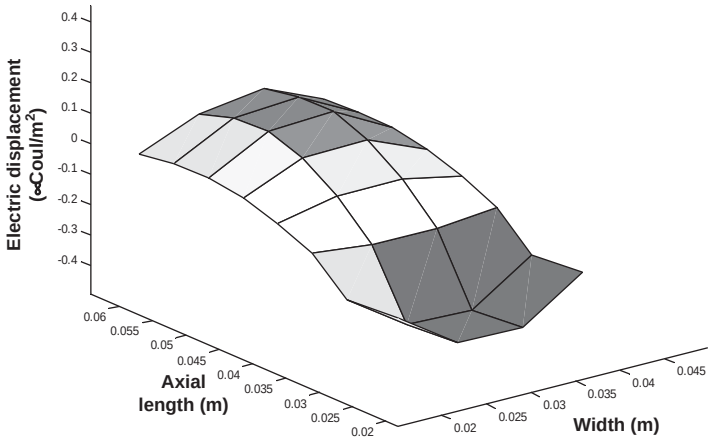

Fig. 11. Electric displacement over the piezoelectric sensor at $t = 60.45\,\mu s$ during impulse loading.

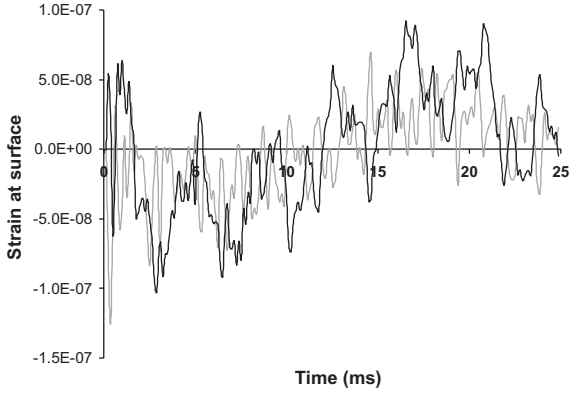

Fig. 12. Longitudinal strain at the plate surface on ends of the PZT patch; edge nearest to the tip (——) and edge closest to the root (——).

across the PZT patch, which leads to the difference in results predicted by the coupled and uncoupled models. The above results are for cross-ply laminates, but similar results are obtained for angle-ply laminates.

4. Experimental comparison

To validate the model and verify the conclusions made from comparison of the coupled theory with the uncoupled approach, a set of experiments was performed. The objective of these experiments was to provide a set of transient sensor outputs for a well-defined model and compare these directly with the results predicted by the developed model.

The test specimen used was a cantilevered plate with two piezoelectric patches bonded to the surface. The plate was made from 3.18 mm thick Aluminum 2024-T3 and the plate geometry is that shown in Fig. 13. The small piezoelectric patch at the root was a custom ACX (Active Control eXperts, Inc.) actuator with wafer dimensions of 1.27 cm length, 0.635 cm width and 0.25 mm thickness. The large piezoelectric patch was an ACX QP-10N actuator with wafer dimensions of 4.597 cm length, 2.057 cm width and 0.25 mm thickness. Both devices were made of PZT-5A with a polyamide coating. The material properties for the aluminum and the piezoelectric devices are shown in Table 2.

The small patch at the root was used as an actuator to induce vibration in the plate, while the larger patch was used as a sensor. To simulate an impulse loading in the plate, a single cycle of high frequency voltage was applied to the actuator. The single cycle voltage was generated by a function generator set to operate in burst mode and create a 3.75 V signal once every 2 s. The input voltage was then amplified to a 75 V-peak signal that was sent to the actuator. This signal is illustrated in Fig. 14.

The sensor output was measured using two different methods. First, the sensor was connected to a charge amplifier that converted the charge flow of the device into a voltage signal that was measured and analyzed using an oscilloscope. This method allowed measurement of the charge

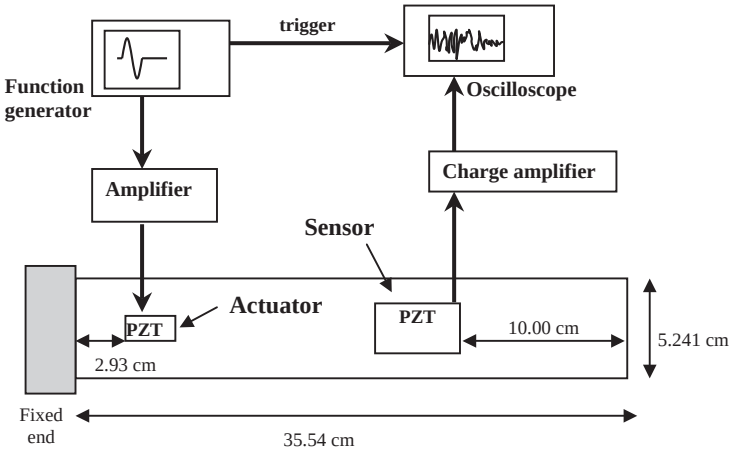

Fig. 13. Plate geometry for transient analysis.

Table 2
Material properties for experimental comparison

Material property	Aluminum	PZT
E (GPa)	68.5	60.6
v	0.326	0.29
G (GPa)	25.83	23.49
ρ (kg/m^3)	2784	7500
d_{31}, d_{32} (m/V)	n/a	-274×10^{-12}
d_{24}, d_{15} (m/V)	n/a	741×10^{-12}
e_3^S (F/m)	n/a	3.01×10^{-9}

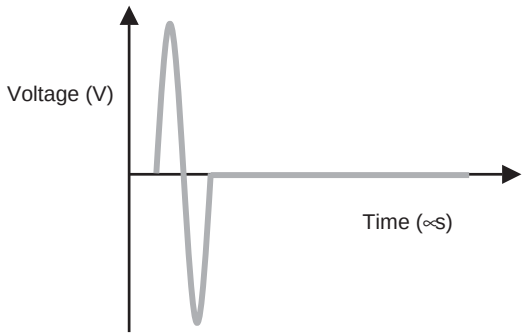

Fig. 14. Input voltage used to simulate impulse loading.

output of the piezoelectric device for comparison with the developed model. Next, the sensor was connected directly to the oscilloscope and the voltage output was measured.

Sensor output was measured for a range of input frequencies. The frequency of the single cycle voltage input allowed control of the duration of the impulse. Higher frequency inputs acted like short duration impulse loads and excited high frequency responses from the system. This method proved to be much more controlled than mechanical impulse loads and the output signals for the impulses were very repeatable. To minimize any effects of noise and deviation between individual impulses, the oscilloscope was set to provide an averaged output using 16 impulse signals.

The charge output for 10, 25 and 50 kHz input frequencies is shown in Fig. 15. The important aspect to be noted from these results is that the overall shape of the output is the same for all three frequencies. The effect of electrical inductance discussed above can be clearly seen, in that it filters high frequency components out of the sensor output. Fig. 16 shows the voltage output for 1, 10 and 25 kHz input frequencies. It is clear by comparing the sensor charge flow in Fig. 15b to the sensor voltage in Fig. 16c that the voltage measurement is more sensitive to high frequency vibration and less affected by the electrical inductance. This is reasonable since although the oscilloscope is not a true open circuit it has a 1 MΩ internal resistance that limits the electrical system to very small net charge flows. Less charge flow in turn implies less effect from inductance, but charge flow within the piezoelectric device during high frequency vibration is still affected.

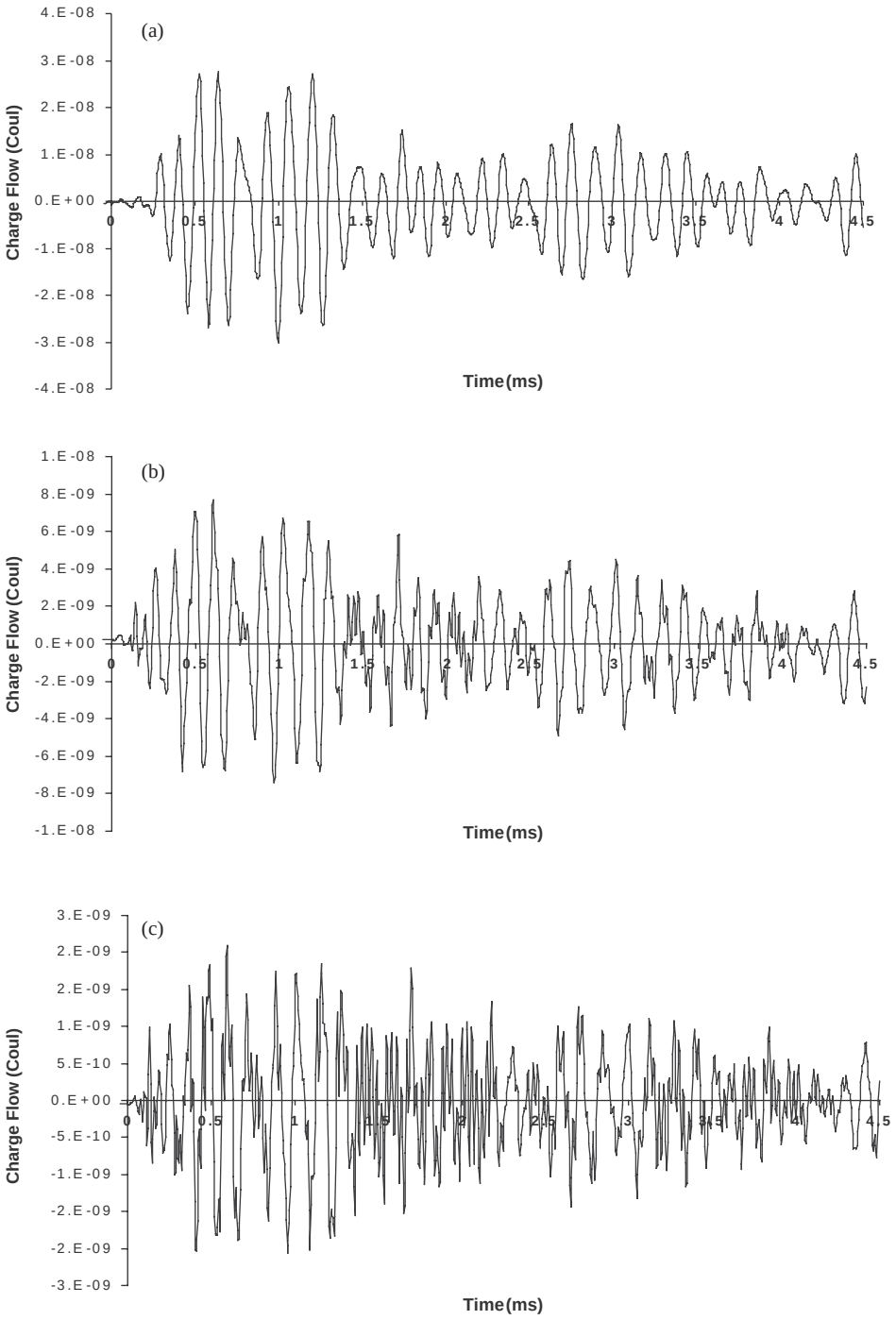

Fig. 15. Sensor charge flow for input frequencies of (a) 10 kHz, (b) 25 kHz and (c) 50 kHz.

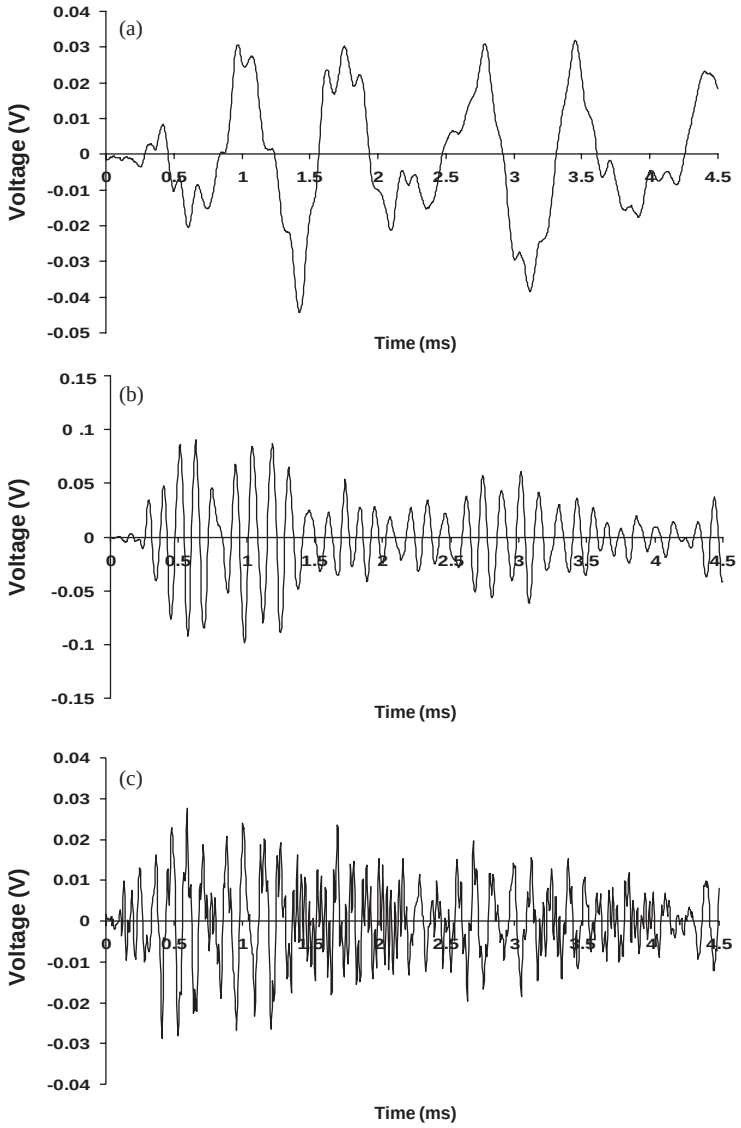

Fig. 16. Sensor voltage for input frequencies of (a) 1 kHz, (b) 10 kHz and (c) 25 kHz.

The developed analysis was used to model the system described above. A finite element mesh with 85 by 9 elements was used for the plate resulting in 860 nodes. The system had 6020 mechanical degrees of freedom, 8 nodal electrical displacements for the small actuator and 48 nodal electrical displacements for the sensor. The material properties listed in Table 2 are used to model the system. First, the natural frequencies of the test specimen were compared with those predicted by the developed model. The natural frequencies of the out-of-plane vibration modes for the case of the sensor being open-circuited are shown in Table 3. There is good comparison for both the bending and twisting modes. However, it should be noted that above 6 kHz mixed mode behavior was mostly observed, and there was less clear correlation between the model and the

Table 3
Vibrational natural frequencies with the sensor open-circuited

Mode	Experiment	Model
Bending 1	20.170	20.326
Bending 2	127.98	128.68
Twisting 1	267.43	267.94
Bending 3	360.10	360.48
Bending 4	702.34	703.58
Twisting 2	821.72	821.40
Bending 5	1164.5	1168.7
Twisting 3	1379.8	1381.7
Bending 6	1744.7	1750.2
Twisting 4	2000.0	2004.5
Bending 7	2434.0	2444.3
Twisting 5	2677.8	2680.5
Bending 8	3235.9	3261.2
Twisting 6	3403.1	3405.9
Bending 9	4114.5	4187.7
Twisting 7	4254.1	4229.7
Bending 10	5236.4	5223.3

Table 4
Vibrational natural frequencies with the sensor electrically shorted

Mode	Experiment	Model
Bending 1	20.147	20.323
Bending 2	127.56	128.45
Twisting 1	267.13	267.94
Bending 3	359.51	359.63
Bending 4	701.09	703.56
Twisting 2	821.36	821.39

experiment. To illustrate the influence of the electrical circuit vibration of the system, the natural frequencies were also computed for the case of the sensor being electrically shorted and are shown in Table 4. When the electrodes of the sensor are shorted, the piezoelectric device cannot store as much electrical energy. This causes the piezoelectric sensor to be less mechanically stiff, thus lowering the natural frequencies of the system. This effect is observed in both the experimental data and the results of the model, however uncoupled approaches are not able to capture this effect.

Overall the model showed a reasonably good ability to predict the transient response of the experimental system. The sensor charge flow predicted by the model for the 25 kHz input frequency is shown in Fig. 17 for both the coupled and uncoupled models. As discussed above, the uncoupled model neglects the electrical inductance and resistance in the electrical circuit and in the piezoelectric devices. This results in large amounts of high frequency content in the predicted response compared to the uncoupled model and the experimental data. Although this can be

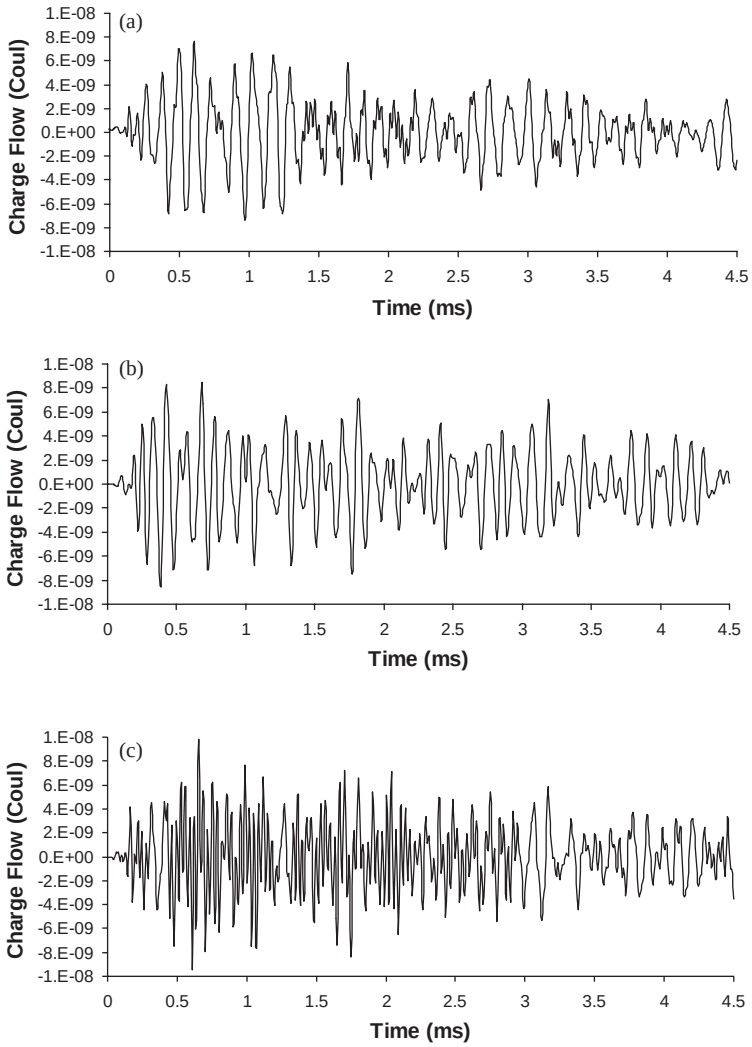

Fig. 17. Sensor charge flow for 25 kHz input frequency from (a) experimental measurement, (b) coupled model and (c) uncoupled model.

observed in Fig. 17, a more valuable comparison can be made by examining the response in the frequency domain. Fig. 18 shows the frequency content of the response for the coupled and uncoupled approaches in comparison to the experimental data. Both models correlate reasonably well at low frequencies, but the uncoupled model has a large amount of high frequency content above 20 kHz.

The variations observed are not unreasonable considering the difficulties associated with accurate modelling of high frequency structural dynamics. The deviation between the experimental data and the coupled model results from a number of factors. One is a limitation of the finite element method and the mesh size used in this model. Another is the classical damping model used for the mechanical damping of the system. Also, since the coupled model includes the

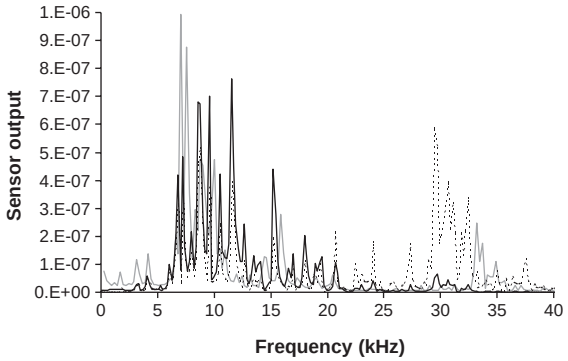

Fig. 18. Frequency domain comparison for 25 kHz input frequency between the experimental data (——), coupled model (——), and uncoupled model (- - - - -).

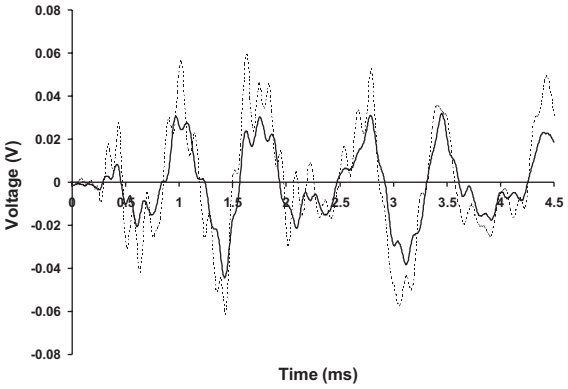

Fig. 19. Predicted response for 1 kHz input frequency; experimental (——) and model (- - - - -).

electrical effects, it is necessary to quantify the electrical resistance and inductance in the electrical circuit and the piezoelectric devices. In this work they were approximated from manufactures' data and simple electrical theory, but it may be necessary to develop more rigorous methods to characterize the electrical aspects of the system.

Next sensor voltage is calculated using the developed model. The sensor voltages predicted by the model for 1 and 10 kHz input frequencies are shown in Figs. 19 and 20. The output is similar to the experimental data, but is less accurate than the predicted charge flow. The reason for this difference is again the difficulty in accurately characterizing the electrical system. The oscilloscope used to measure the voltage experimentally is not an ideal voltage-measuring device. The actual circuit measures the voltage across a large resistor and the circuit has a small amount of charge flow, contrary to the zero net charge flow assumed by the piezoelectric boundary conditions. Also, the charge flow within the PZT becomes extremely important in determining the output voltage. A more detailed characterization of the internal inductance and resistance of the piezoelectric device and voltage measuring circuit must be used to accurately model the voltage response of an adaptive structure.

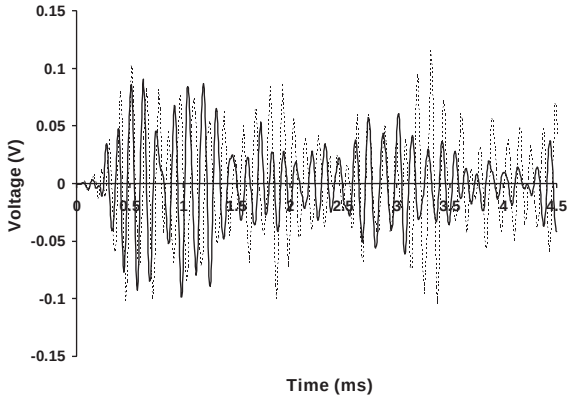

Fig. 20. Predicted response for 10 kHz input frequency; experimental (——) and model (- - - - -).

5. Conclusions

A new approach has been developed for modelling the transient response of composite laminates with piezoelectric sensors and actuators. The mathematical model uses a coupled piezoelectric-mechanical theory that accurately captures both electrical and mechanical characteristics of adaptive structures. Parametric studies were performed to assess the difference in results predicted between the refined higher-order laminate theory and the classical plate theory, as well as between the coupled and uncoupled piezoelectric models. Comparison with experimental data showed that the developed model gives good results, although the results are sensitive to the internal inductance of the piezoelectric device. The following conclusions were made from the present study

(1) For thin plates, the differences in mechanical displacements predicted by the higher-order and the classical plate theories are significant only when the time step is sufficiently small to capture very high frequency modes. The differences in sensor output are more significant in all cases.
(2) For thicker plates, significant differences are observed in both mechanical displacements and sensor output predicted by the higher-order and the classical plate theories.
(3) Although moderate differences are observed in the predictions of mechanical displacements, larger differences are observed for both charge and voltage measurements, predicted by the coupled and uncoupled models.
(4) The assumption of constant electric field over the entire PZT area in the uncoupled theory leads to inaccuracies in modelling the effect of high frequency vibrations that create both areas of local compression and local tension within the PZT patch.

Acknowledgements

This research was supported by the Air Force Office of Scientific Research, Technical monitor, Daniel Segalman.

References

[1] E.F. Crawley, Use of piezoelectric actuators as elements of intelligent structures, *American Institute of Aeronautics and Astronautics Journal* 25 (1987) 1373–1385.
[2] D.T. Detwiler, M.H. Shen, V.B. Venkayya, Finite element analysis of laminated composite structures containing distributed piezoelectric actuators and sensors, *Finite Elements in Analysis and Design* 20 (1995) 87–100.
[3] H.F. Tiersten, Hamilton's principle for linear piezoelectric media, *IEEE Proceedings* 55 (1967) 1523–1524.
[4] N.W. Hagood, A. Von Flotow, Damping of structural vibrations with piezoelectric materials and passive electrical networks, *Journal of Sound and Vibration* 146 (1991) 243–268.
[5] S.Y. Wu, Piezoelectric shunts with a parallel *R–L* circuit for structural damping and vibration control, *Smart Structures and Materials 1996: Passive Damping, Proceedings of the International Society for Optical Engineering* 2720 (1996) 259–269.
[6] E.H. Anderson, N.W. Hagood, Simultaneous piezoelectric sensing/actuation: analysis and application to controlled structures, *Journal of Sound and Vibration* 174 (1994) 617–639.
[7] J.A. Mitchell, J.N. Reddy, A refined hybrid plate theory for composite laminates with piezoelectric laminae, *International Journal of Solids Structure* 32 (1995) 2345–2367.
[8] A. Chattopadhyay, J. Li, H. Gu, A coupled thermo-piezoelectric-mechanical model for smart composite laminates, *American Institute of Aeronautics and Astronautics Journal* 37 (1999) 1633–1638.
[9] R.P. Thornburgh, A. Chattopadhyay, Simultaneous modeling of mechanical and electrical response of smart composite structures, *American Institute of Aeronautics and Astronautics Journal* 40 (2002) 1603–1610.
[10] J.N. Reddy, A simple higher-order theory for laminated composite plates, *Journal of Applied Mechanics* 51 (1984) 745–746.
[11] K.J. Bathe, *Finite Element Procedures*, Prentice Hall, Englewood Cliffs, NJ, 1996.